

Heritability Analysis with Repeat Measurements: Application to Resting-state Functional Connectivity

Tian Ge^{a,b,c}, Avram J. Holmes^{a,d,e}, Randy L. Buckner^{a,e,f}, Jordan W. Smoller^{b,c,*}, Mert R. Sabuncu^{a,g,h,*}

^aAthinoula A. Martinos Center for Biomedical Imaging, Massachusetts General Hospital / Harvard Medical School, Charlestown, MA 02129, USA; ^bPsychiatric and Neurodevelopmental Genetics Unit, Center for Human Genetic Research, Massachusetts General Hospital, Boston, MA 02114, USA; ^cStanley Center for Psychiatric Research, Broad Institute of MIT and Harvard, Cambridge, MA 02138, USA; ^dDepartment of Psychology, Yale University, New Haven, CT 06520, USA; ^eDepartment of Psychiatry, Massachusetts General Hospital / Harvard Medical School, Boston, MA 02114, USA; ^fDepartment of Psychology and Center for Brain Science, Harvard University, Cambridge, MA 02138, USA; ^gComputer Science and Artificial Intelligence Laboratory, Massachusetts Institute of Technology, Cambridge, MA 02139, USA; ^hSchool of Electrical and Computer Engineering and School of Biomedical Engineering, Cornell University, Ithaca, NY 14853, USA.

*MRS and JWS contributed equally to this work.

Emails: tge1@mgh.harvard.edu (TG); msabuncu@nmr.mgh.harvard.edu (MRS)

Abstract

Heritability, defined as the proportion of phenotypic variation attributable to genetic variation, provides important information about the genetic basis of a trait. Existing heritability analysis methods do not discriminate between *stable* effects, e.g., due to the subject's unique environment, and *transient* effects, such as measurement error. This can lead to misleading assessments, for example, when comparing the heritability of traits that exhibit different levels of reliability. Here, we present a linear mixed effects model to conduct heritability analyses that explicitly account for intra-subject fluctuations (e.g., due to measurement noise or biological transients) using repeat measurements. We apply the proposed strategy to the analysis of resting-state functional MRI (rs-fMRI) measurements — a prototypic data modality that exhibits variable levels of test-retest reliability across space. Our results, for the first time, show that the stable components of functional connectivity within and across well-established large-scale brain networks can be considerably (as high as 90%) heritable. Furthermore, we demonstrate that dissociating intra- and inter-subject variation can reveal genetic influences on a phenotype that cannot be captured by conventional heritability analyses.

Significance

Heritability quantifies the proportion of genetic influence on the variation of a trait, and is a fundamental metric in population genetics. Existing heritability models lump together *stable* effects, e.g., due to the subject's unique environment, and *transient* effects, such as measurement error. This can result in the underestimation of heritability and misleading assessments when comparing the heritability of traits that exhibit different levels of reliability. This paper presents an analytic strategy that can account and correct for transient intra-subject variation using repeat measurements when investigating the heritability of a phenotype. Using the proposed method, we show, for the first time, that the stable components of functional connectivity within and across well-established large-scale brain networks can be considerably heritable. With the explosive expansion of genomics, health informatics and digital phenotyping technologies, the proposed model will be significant in dissecting the genetic basis of a wide range of novel, informative but noisy phenotypes such as gene expression, wearable sensor data, and web-based cognitive and behavioral assessments.

Introduction

Heritability of a trait is defined as the proportion of phenotypic variation that can be explained by genetic variation among individuals in a population [Visscher et al., 2008]. It is a fundamental concept in population and statistical genetics, providing basic but important information about the genetic underpinnings of a trait. The heritability of a large number of human complex traits across a wide range of the phenotypic spectrum has been documented, using classical twin or pedigree designs [Falconer, 1960; Neale and Cardon, 1992; Almasy and Blangero, 1998; Polderman et al., 2015], or statistical methodologies developed more recently that allow for the estimation of heritability in large samples of unrelated subjects [Yang et al., 2010, 2011; Golan et al., 2014; Ge et al., 2015, 2016a,b].

All statistical models for heritability analysis include an error term (residual) that absorbs the phenotypic variation that cannot be explained by genetics and common environment. The residual therefore accounts for unique (subject-specific) environmental effects, measurement error, and intra-subject fluctuation of the trait of interest due to, for example, biological cycles such as the circadian rhythm. With one measurement for each subject, these factors cannot be dissociated and are typically modeled jointly as an independent and identically distributed (i.i.d.) random variable across subjects. However, this model imposes at least two problems on heritability analysis. First, measurement error has a ceiling effect on heritability estimates; it inflates the total phenotypic variation and downwardly biases heritability estimates. Second, comparing the heritability of traits that have different levels of measurement noise may be misleading.

The issues can be partially resolved if repeat measurements of a trait are available. Assuming that multiple repeat measurements have been collected for each subject over a period of time in which we expect little biologically meaningful change to the trait (i.e., the genetic architecture of the trait and the environmental influences remain largely unchanged during the time period), we can then distinguish factors that contribute to the inter-subject variation of the phenotype but are stable across repeat measurements (e.g., due to unique environmental effects) from factors that exhibit intra-subject fluctuation (e.g., measurement error). Defining heritability as the fraction of the total stable inter-subject variation that is attributable to genetic variation removes the ceiling effect of measurement error and makes the heritability estimates of traits that have different levels of noise comparable. To date, repeat measurements have not been used this way in heritability estimation. Instead, serial measurements are typically averaged, yielding one scalar measurement for each subject such that conventional heritability analysis methods can be applied. Although averaging repeat measurements cancels out some measurement error and thus improves the reliability of the phenotype, it does not dissociate

intra- and inter-subject variation and can still lead to the underestimation of the heritability of a trait in the presence of noise.

In this paper, we present a linear mixed effects (LME) model that can leverage repeat measurements to explicitly dissociate intra- and inter-subject variation of a phenotype, and compute heritability with respect to stable inter-subject variation. As a demonstration of application, we investigate the heritability of (intrinsic) functional connectivity measurements derived from resting-state functional MRI (rs-fMRI). rs-fMRI is a prototype case where a substantial amount of measurement noise from multiple sources (including thermal, system and physiological) often exists in the data [Krüger and Glover, 2001; Triantafyllou et al., 2005]. Long-range functional connectivity computed from rs-fMRI time series might span distant brain regions that have dramatically different levels of measurement error due to the complex spatial pattern of the noise and susceptibility artifacts. Moreover, the brain is a dynamic system where time-varying fluctuations in functional connectivity and brain networks, and transitions between different brain states have been observed [Hutchinson et al., 2013]. Therefore, part of the variation in rs-fMRI-derived measurements can be attributed to a non-transient component for each subject, while the remaining variation might be due to transient neuronal activities or mind-wandering, and can change between scanning sessions of a subject. Recent studies have also shown that individual differences in functional connectivity are heterogeneous across the cortex after accounting for intra-subject variation, with larger variability in high-level association cortex (e.g., the lateral prefrontal cortex and the temporal-parietal junction) and smaller variability in unimodal regions (e.g., the motor and somatosensory cortex), pointing to a potential relationship between the spatial distribution of inter-subject variation in functional connectivity and brain evolution and development [Mueller et al., 2013]. Disentangling the non-transient, stable component of rs-fMRI measurements from the transient signal across repeat scans (e.g., measurement error), and estimating the stable heritability might thus improve our understanding of the genetic basis of brain function.

Although a handful of studies have investigated the genetic basis of the functional connectome and functional brain networks [Glahn et al., 2010; Fornito et al., 2011; Thompson et al., 2013], to the best of our knowledge, none have addressed intra- and inter-subject variation of rs-fMRI measurements, despite the fact that repeat scans are commonly collected in rs-fMRI studies. Here, using rs-fMRI data collected by the Human Connectome Project (HCP) [Van Essen et al., 2013] and the Harvard/Massachusetts General Hospital (MGH) Brain Genomics Superstruct Project (GSP) [Holmes et al., 2012, 2015], we demonstrate that (1) the relative contributions of intra- and inter-subject variation to the total variation of rs-fMRI-derived functional connectivity measurements are dramatically different across space and strongly correlated with test-retest reliability;

(2) the stable components of functional connectivity (within and between functional brain networks) can be substantially heritable; and (3) dissociation of intra- and inter-subject variation can reveal genetic influences on the functional architecture of the human brain that are not detectable by conventional heritability analyses. Our results provide novel insights into the genetic basis of brain function and highlight the importance of accounting for the spatial pattern of measurement noise and transient signals when studying the heritability of functional connectivity measurements across brain regions.

Results

We first conducted simulation studies to ensure that our proposed LME model can robustly dissociate intra- and inter-subject variation of a phenotype and accurately estimate heritability due to inter-subject variation using repeat measurements. We simulated phenotypes using real HCP covariates, family structure, and number of repeat measurements, and the heritability due to inter-subject variance was set to 80% (see Methods). When different levels of intra-subject measurement-to-measurement variation (ranged from 10% to 80% of the total phenotypic variance) was added to the phenotype, our proposed method (Fig. 1, black) consistently produced unbiased estimates of the heritability attributable to inter-subject variation. Conversely, the classical ACE model (Fig. 1, red; A: additive genetics; C: common environment; E: unique environment) cannot explicitly dissociate intra- and inter-subject variation, and ACE heritability estimates decreased as intra-subject variation (and also total phenotypic variation) increased.

We then sought to characterize the spatial distribution of intra- and inter-subject variation of functional connectivity measurements using real rs-fMRI data collected by the HCP and GSP Consortium. Specifically, we analyzed 584 young and healthy subjects (72 monozygotic twin pairs, 67 dizygotic twin pairs, 251 full siblings of twins and 55 singletons) from the HCP and 809 unrelated young and healthy subjects from the GSP. A previously published and widely validated rs-fMRI-based parcellation of 7 cortical functional networks (visual, somatomotor, dorsal attention, ventral attention/salience, limbic, control and default network) [Yeo et al., 2011] was split into 51 spatially contiguous regions across the two hemispheres (Fig. 2A). For each rs-fMRI scan, spatially normalized Pearson correlation coefficients between preprocessed time series at pairs of cortical regions were summarized within and across these network regions into a 51×51 matrix (see Methods). When averaging across scans, the functional connectivity matrices computed from both the HCP and the GSP sample showed clear modular structures (Fig. 2B). In particular, negative correlations between attention networks and the default mode network (DMN) can be clearly observed.

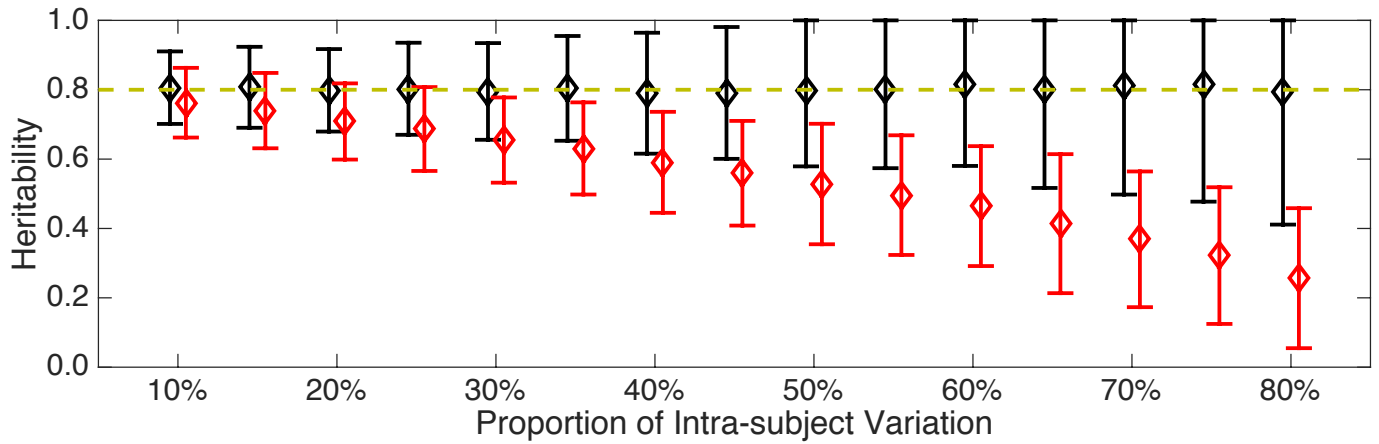


Figure 1: **Results of simulation studies.** Phenotypes were simulated using real HCP covariates, family structure, and number of repeat measurements. The heritability due to inter-subject variation was 80%. The proposed heritability analysis method (black) and the classical ACE model (red) were used to estimate heritability when different levels of intra-subject measurement-to-measurement variation (ranged from 10% to 80% of the total phenotypic variance) was added to the phenotype. The simulation was repeated 1,000 times for each level of intra-subject variation. The average heritability estimates and empirical standard errors of point estimates are shown.

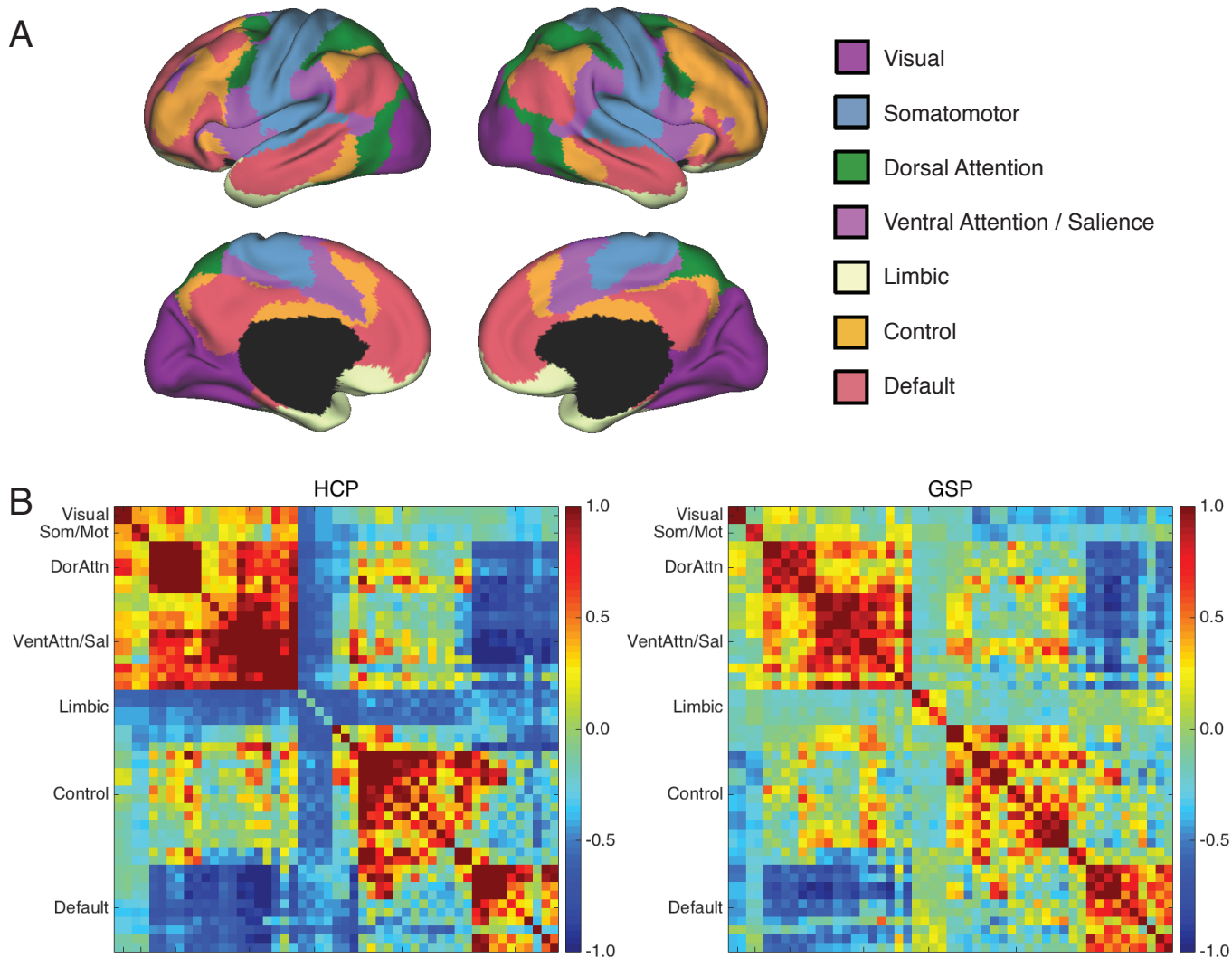


Figure 2: Functional connectivity measurements between pairs of 51 brain regions. (A) Surface representation of the 7-network parcellation [Yeo et al., 2011], which can be split into 51 spatially contiguous regions across the two hemispheres. (B) Average functional connectivity measurements between pairs of the 51 brain regions across scans in the HCP sample (left) and GSP sample (right). Regions belong to the same functional network are grouped together in the visualization.

We fit the proposed LME model that partitions the total phenotypic variation into inter-subject variation (the stable, non-transient component) and intra-subject variation (including the unstable, transient component and measurement error), using the 51×51 functional connectivity matrices computed for each rs-fMRI session in the HCP sample. Figure 3A shows that the relative contributions of intra- and inter-subject variation are highly heterogeneous across space. The spatial pattern of inter-subject variation is similar to and highly correlated with (Pearson's $r = 0.838$) the test-retest reliability of functional connectivity measurements estimated using a subset of the HCP sample that were sampled from different families and had repeat rs-fMRI scans (Fig. 3B and 3C, left). The inter-subject variation estimated in HCP also agrees with the test-retest reliability of functional connectivity measurements estimated using the independent GSP sample (Pearson's $r = 0.528$; Fig. 3B and 3C, right). Within-network functional connectivities show larger inter-subject variation and higher test-retest reliability than between-network connectivities in general. Yet there are certain exceptions, such as the connectivity between the control and default network, which is also highly reliable. There is strong agreement between the spatial patterns of test-retest reliability estimated using the HCP and GSP sample.

The heritability of the stable, non-transient component of rs-fMRI-derived functional connectivity measurements, defined as the proportion of inter-subject variation attributable to the genetic variation in the population, is substantial for many pairs of brain regions (Fig. 4, right), and is consistently higher than conventional heritability estimates (the proportion of the total phenotypic variation attributable to genetic variation; Fig. 4, left) computed by averaging repeat measurements for each individual and applying the classical ACE model. Overall, within-network functional connectivity measurements for all of the 7 functional networks are significantly heritable, but the non-transient heritability estimates are consistently larger than the conventional heritability estimates (Fig. 4B).

Lastly, we carried out an analysis of the functional connectivity profile of the posterior cingulate cortex (PCC) seed, a core region of the DMN, in the HCP sample. As is well-known, the PCC is strongly positively correlated with other regions in the DMN such as the medial prefrontal cortex, inferior parietal lobule and lateral temporal cortex, while negatively correlated with the dorsal and ventral attention networks (Fig. 5A). Functional connectivities within the DMN show high test-retest reliability and low intra-subject variation, while regions not coupled with the PCC such as the motor and somatosensory cortex and visual cortex show lower test-retest reliability and higher intra-subject variation (Fig. 5B and Fig. 5F). The heritability maps of the functional connectivity profile estimated by the classical ACE model (Fig. 5C) and the proposed LME model (Fig. 5D) have similar patterns in general; both clearly show that functional connectivities within

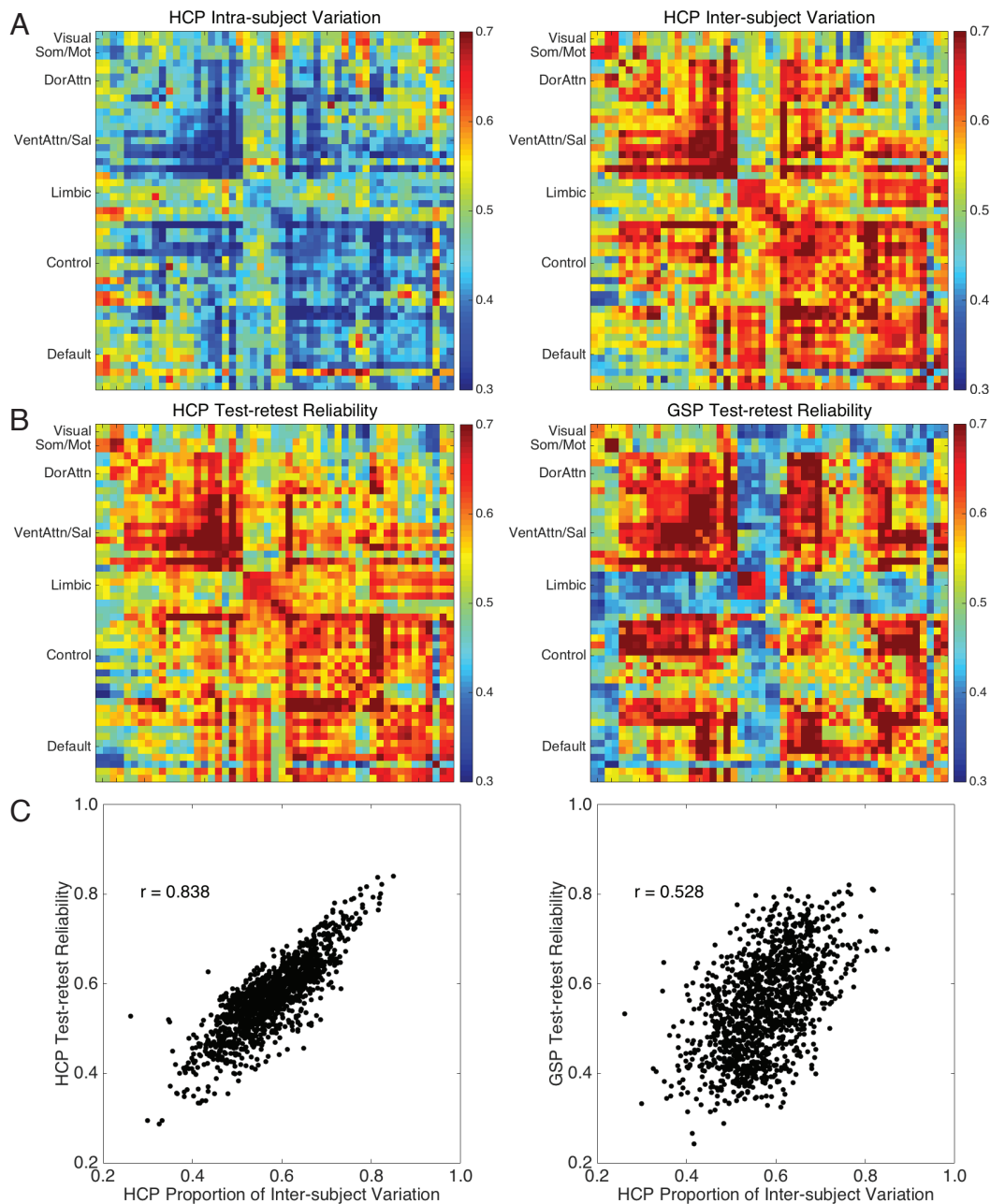


Figure 3: Intra- and inter-subject variation of the resting-state functional connectivity measurements. (A) Proportion of the total phenotypic variation attributable to intra-subject measurement-to-measurement variation (left) and stable, non-transient inter-subject variation (right) estimated in the HCP sample. (B) Test-retest reliability of the functional connectivity measurements estimated using the HCP sample (left) and GSP sample (right). (C) Test-retest reliability of the functional connectivity measurements estimated in the HCP (left) and GSP (right) sample plotted against the proportion of phenotypic variance explained by the inter-subject variation estimated in the HCP sample.

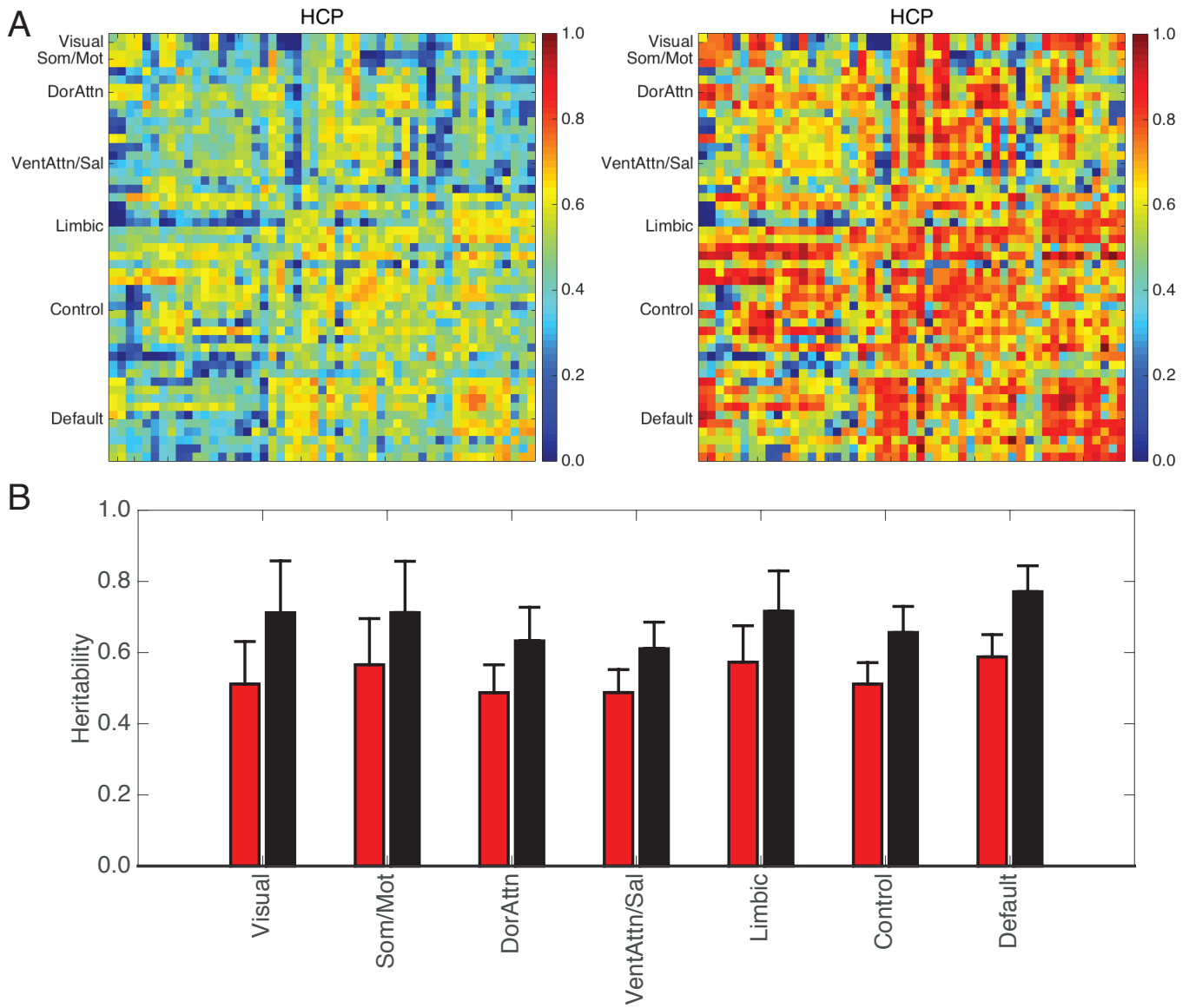


Figure 4: **Heritability of functional connectivity measurements.** (A) Conventional heritability estimates of functional connectivity measurements computed by averaging repeat measurements for each subject and applying the classical ACE model (left), and the heritability estimates of the stable, non-transient component of functional connectivity, (i.e., the proportion of the inter-subject variation due to genetic variation) computed using the proposed linear mixed effects model (right). (B) Average of the heritability estimates of within-network functional connectivity measurements for each of the 7 functional networks. Heritability was estimated using the proposed method (black) and the classical ACE model (red). The standard errors shown were estimated by a block-jackknife procedure.

the DMN are highly heritable. Contrasting the two heritability maps reveals that the proposed LME method produces substantially higher heritability estimates than the classical ACE model in the attention networks and the visual cortex (Fig. 5E), indicating that the functional connectivities between PCC and these regions are under significant genetic influences after accounting for the unstable, transient signal in functional connectivity measurements.

Discussion

In this paper, we presented a LME model that can explicitly dissociate stable, non-transient inter-subject variation (e.g., due to long-lasting unique environmental effects) and transient, intra-subject measurement-to-measurement variation (e.g., due to measurement noise) of a phenotype using repeat measurements. By defining non-transient heritability as the proportion of (stable) inter-subject variation that can be explained by genetic variation, we can correct for the effect of intra-subject fluctuations such as measurement error on heritability estimates, and put phenotypes with different levels of measurement noise on equal footing to assess their comparative heritability.

The proposed statistical model is a straightforward extension to the classical ACE model, which is widely used in heritability analysis. Specifically, in addition to the additive genetic, common environmental and unique environmental effects, a random effect that captures intra-subject variation is included in the model. With repeat measurements, these random effects have different covariance structures and thus the model is identifiable and can be fitted using established statistical methods such as the restricted maximum likelihood (ReML) estimation [Patterson and Thompson, 1971; Harville, 1977; Lindstrom and Bates, 1988]. Similar attempts to correct for measurement error in heritability analysis with repeat measurements were made in twin studies using structural equation modeling [Kendler et al., 1999].

Although we demonstrated our method using an extended twin sample collected by the HCP, the model can be easily applied to heritability analysis in unrelated samples, where the genetic similarity matrix is empirically estimated from genome-wide genetic variants such as single nucleotide polymorphisms (SNP) [Yang et al., 2010, 2011], and the common environment matrix is often assumed to vanish. It is worth mentioning that in unrelated subject studies heritability estimates only capture genetic variation assayed by genotyping microarrays (known as SNP heritability), and thus should be interpreted differently from the classical narrow-sense heritability estimated from twin or family studies [Visscher et al., 2008].

The proposed method can be applied to any phenotype on which repeat measurements are available. In

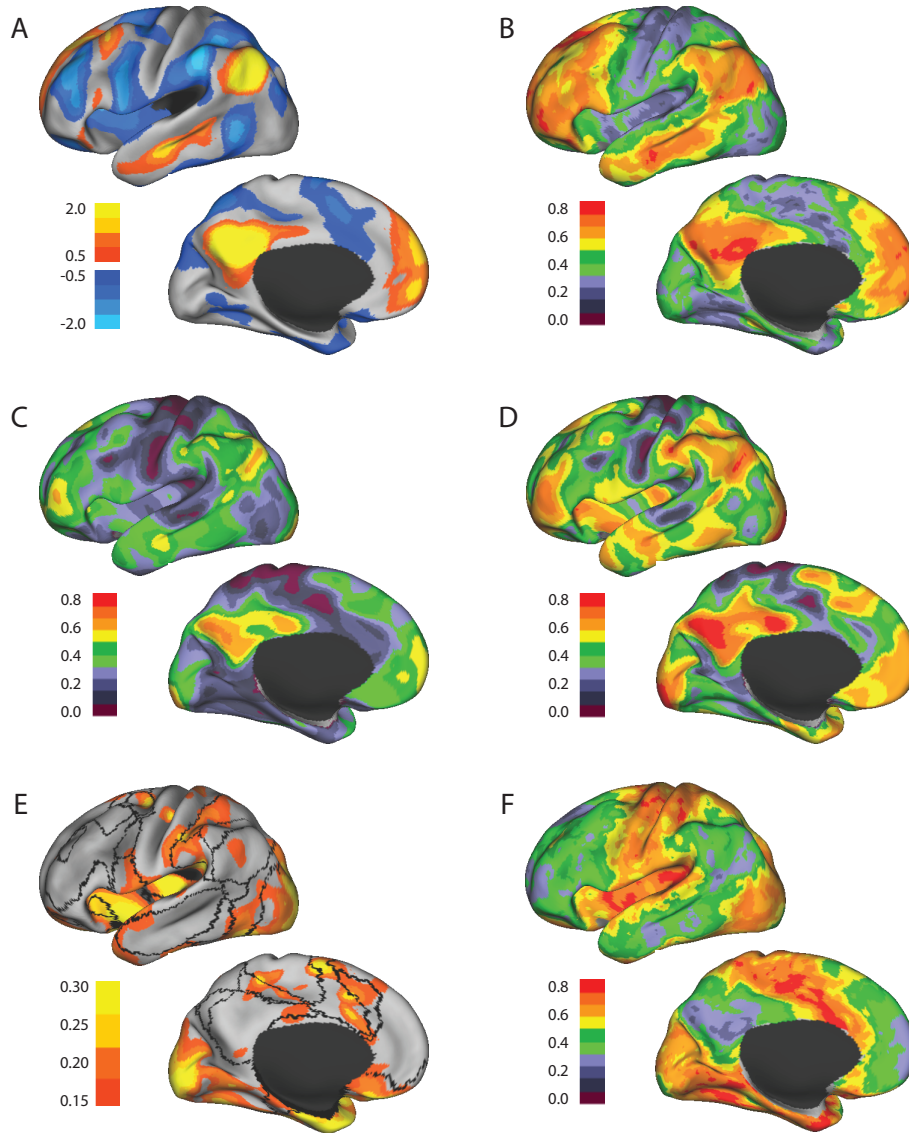


Figure 5: **Analysis of the functional connectivity profile seeded at posterior cingulate cortex (PCC) in the HCP sample.** (A) Average functional connectivity profile across subjects. (B) Test-retest reliability of the functional connectivity profile estimated using an unrelated subset of the HCP sample. (C) Heritability estimates of the functional connectivity profile computed using the classical ACE model. (D) Heritability estimates of the stable, non-transient component of the functional connectivity profile computed using the proposed method. (E) Difference of the heritability estimates computed by the proposed model and the classical ACE model, with the boundaries of the 7 functional networks overlaid. (F) Proportion of the total phenotypic variation attributable to intra-subject measurement-to-measurement variation.

particular, with the explosive expansion of genomics, health informatics and deep phenotyping technology, the proposed model has the potential to dissect the genetic basis of a wide range of novel, informative but noisy phenotypes such as gene expression, wearable sensor data, and web-based cognitive and behavioral assessments. We have used functional connectivity measurements computed from rs-fMRI as an example because repeat scans are often collected in fMRI studies, and it is known that rs-fMRI features often contain substantial amount of noise from multiple sources and typically have lower test-retest reliability than morphological measurements derived from structural brain MRI scans. We confirmed that for some functional connectivity measures more than 70% of the phenotypic variation can be attributed to transient intra-subject variation. More importantly, the contribution of the stable, non-transient component of functional connectivity to the total phenotypic variation varies dramatically across space and is strongly correlated with the test-retest reliability of the measurements. For example, connectivity measurements between the limbic network (e.g., the temporal pole and orbito-frontal regions) and other brain regions have much smaller stable inter-subject components and relatively lower test-retest reliability [Holmes et al., 2015], likely due to susceptibility artifacts associated with sinus and temporal bone regions [Deichmann et al., 2003; Weiskopf et al., 2006]. Head motion might also have systematic influences on rs-fMRI-derived measurements and exert differential effects on distant and regional functional couplings [Power et al., 2012; Van Dijk et al., 2012; Satterthwaite et al., 2012]. The heterogeneous distribution of the spatial noise and confounds in rs-fMRI underscores the importance of accounting and correcting for intra-subject variation when comparing the heritability of functional connectivity measurements across space. Moreover, although the reliability of rs-fMRI signals depends on the scanner type and imaging sequence, we observed largely consistent spatial patterns of test-retest reliability between the HCP and GSP samples, suggesting that a large portion of the measurement-to-measurement variation might be dominated by factors shared across imaging sites, scanning protocols and samples.

Previous studies have shown that resting-state functional connectivity measures within the DMN are significantly heritable [Glahn et al., 2010]. Graph theoretical measures that index topological characteristics and communication efficiency of intrinsic brain networks were also found to be heritable in both adults [Fornito et al., 2011] and normally developing children [van den Heuvel et al., 2013]. We have demonstrated in the present study that the stable, non-transient components of rs-fMRI-derived functional connectivity measurements are highly heritable between many brain regions, and all functional networks we examined have substantially heritable within-network couplings. To our knowledge, our analyses provide the first heritability estimates of functional connectivity for multiple brain networks. The heritability analysis of the functional connectivity profile seeded in the PCC, a core region of the DMN [Buckner et al., 2008] that is strongly pos-

itively correlated with other DMN regions including the medial prefrontal cortex, inferior parietal lobule and lateral temporal cortex, further confirmed that functional connectivities within the DMN are under strong genetic influences. Moreover, using the proposed LME model, we identified that several regions that are weakly correlated (e.g., the visual cortex) or negatively correlated with PCC (e.g., the attention networks), exhibit highly heritable non-transient functional couplings with the seed. This is in contrast with the picture offered by a conventional heritability analysis, in which heritability estimates of these weak or negative couplings did not stand out from the background, likely because these regions are not consistently co-activated across subjects during resting state, and the functional connectivity measurements comprise large transient components that vary from scan to scan. Our results thus underscore the importance of accounting and correcting for transient intra-subject variation when investigating the heritability of functional connectivity measurements across space, and indicate that the proposed method has the potential to unveil the genetic basis of the functional connectome that cannot be captured by conventional heritability analyses.

There are some technical limitations of the proposed method that we would like to point out. First, we note that although non-transient heritability estimates defined with respect to stable inter-subject variation are typically larger than conventional heritability estimates where the total phenotypic variation is used for normalization, the statistical power (in terms of testing the significance of heritability) will not necessarily be larger because the proposed model includes one more parameter than the ACE model and thus the uncertainties in the point estimates of variance component parameters might increase. In fact, there may be a substantial power loss when applying the proposed model in a setting of moderate sample size, small number of repeat measurements, and large measurement error. In this case, the classical model is recommended for more robust model fitting and statistical inferences. Furthermore, the standard error on the point estimate of the heritability in the proposed model depends on the sample size, number of repeat measurements and the covariance structure of the phenotype (i.e., the relative contributions of additive genetics, common environment, unique environment and transient noise), and can vary across phenotypes even in the same sample. Finally, it is important to emphasize that the proposed model merely examines stable inter-subject phenotypic variation, while treating temporal variation as a nuisance. In longitudinal settings, such as during development or progressive disease, where the temporal dynamics of a measurement is the phenotype of interest, the proposed strategy will be inappropriate.

Methods

Linear mixed effects modeling. We consider the following linear mixed effects (LME) model for repeat measurements [Laird and Ware, 1982; Verbeke and Molenberghs, 2009]:

$$y_{ij} = \mathbf{x}_{ij}^\top \boldsymbol{\beta} + \gamma_i + \epsilon_{ij}, \quad i = 1, 2, \dots, m, \quad j = 1, 2, \dots, n_i, \quad (1)$$

where m is the total number of subjects; y_{ij} is the j -th repeat measurement from the i -th subject, and the number of repeat measurements n_i can be subject-specific; \mathbf{x}_{ij} is a $q \times 1$ vector, which can incorporate both time-invariant individual-level covariates and time-varying covariates; $\boldsymbol{\beta}$ is a $q \times 1$ vector of unknown fixed (population-level) effects; γ_i is a random intercept, which describes subject-specific deviation from the population mean; and ϵ_{ij} denotes intra-subject measurement-to-measurement variation (e.g., measurement error or the unstable, transient component) of y_{ij} , and is assumed to be independent of the random effects and independent between repeat measurements. We assume that $\boldsymbol{\gamma} = [\gamma_1, \dots, \gamma_m]^\top$ can be partitioned into the sum of additive genetic effect \mathbf{g} , common (or shared) environment \mathbf{c} and unique (subject-specific) environment \mathbf{e} , and their covariance structures take the following forms:

$$\mathbf{g} \sim N(\mathbf{0}, \sigma_A^2 \mathbf{K}), \quad \mathbf{c} \sim N(\mathbf{0}, \sigma_C^2 \boldsymbol{\Lambda}), \quad \mathbf{e} \sim N(\mathbf{0}, \sigma_E^2 \mathbf{I}_m), \quad (2)$$

where $N(\boldsymbol{\mu}, \boldsymbol{\Sigma})$ denotes a multivariate normal distribution with mean $\boldsymbol{\mu}$ and covariance matrix $\boldsymbol{\Sigma}$; σ_A^2 , σ_C^2 and σ_E^2 are the additive genetic variance, common environmental variance and unique environmental variance, respectively; \mathbf{K} is an $m \times m$ genetic similarity matrix, $\boldsymbol{\Lambda}$ is an $m \times m$ matrix that quantifies shared environment between pairs of individuals, and \mathbf{I}_m is an $m \times m$ identity matrix. In familial studies, \mathbf{K} is twice the kinship matrix, $\mathbf{K} = 2\boldsymbol{\Pi}$, and indicates the expected additive genetic covariance among individuals. The ij -th entry of the kinship matrix, ϕ_{ij} , known as the kinship coefficient, defines genetic relatedness for subjects i and j , and in general can be derived from pedigree information. $\boldsymbol{\Lambda}$ usually reflects household sharing between pairs of individuals. In the present study, $\phi_{ij} = 1/2$ for monozygotic (MZ) twins and $\phi_{ij} = 1/4$ for dizygotic (DZ) twins and full siblings, and we assume that twin pairs and their non-twin siblings share the same environment and the corresponding elements in $\boldsymbol{\Lambda}$ are one. We further assume that $\epsilon_{ij} \sim N(0, \sigma_M^2)$.

Using matrix notations $\mathbf{y}_i = [y_{i1}, \dots, y_{in_i}]^\top$, $\mathbf{X}_i = [\mathbf{x}_{i1}, \dots, \mathbf{x}_{in_i}]^\top$, $\boldsymbol{\epsilon}_i = [\epsilon_{i1}, \dots, \epsilon_{in_i}]^\top$, and denoting $\mathbf{1}_{n_i}$ as a column vector of n_i ones, model (1) can be written as

$$\mathbf{y}_i = \mathbf{X}_i \boldsymbol{\beta} + \mathbf{1}_{n_i} \gamma_i + \boldsymbol{\epsilon}_i, \quad i = 1, 2, \dots, m. \quad (3)$$

We can further stack the data from all subjects and write model (3) as

$$\mathbf{y} = \mathbf{X} \boldsymbol{\beta} + \mathbf{T} \boldsymbol{\gamma} + \boldsymbol{\epsilon}, \quad \boldsymbol{\gamma} = \mathbf{g} + \mathbf{c} + \mathbf{e}, \quad (4)$$

where $\mathbf{y} = [\mathbf{y}_1^\top, \dots, \mathbf{y}_m^\top]^\top$, $\mathbf{X} = [\mathbf{X}_1^\top, \dots, \mathbf{X}_m^\top]^\top$, $\mathbf{T} = \text{blkdiag}\{\mathbf{1}_{n_1}, \dots, \mathbf{1}_{n_m}\}$ is a block diagonal matrix of size $n \times m$, $n = \sum_{i=1}^m n_i$ is the total number of measurements, and $\boldsymbol{\epsilon} = [\boldsymbol{\epsilon}_1^\top, \dots, \boldsymbol{\epsilon}_m^\top]^\top$. The covariance matrix of \mathbf{y} can be calculated as

$$\text{cov}[\mathbf{y}] = \mathbf{T} \text{cov}[\boldsymbol{\gamma}] \mathbf{T}^\top + \text{cov}[\boldsymbol{\epsilon}] = \sigma_A^2 \mathbf{T} \mathbf{K} \mathbf{T}^\top + \sigma_C^2 \mathbf{T} \boldsymbol{\Lambda} \mathbf{T}^\top + \sigma_E^2 \mathbf{T} \mathbf{T}^\top + \sigma_M^2 \mathbf{I}_n. \quad (5)$$

We then define the non-transient heritability of a trait as the proportion of the total stable, non-transient inter-subject variation that can be explained by genetic variation in the population:

$$h^2 = \frac{\sigma_A^2}{\sigma_A^2 + \sigma_C^2 + \sigma_E^2}. \quad (6)$$

Unbiased estimates of the unknown variance component parameters σ_A^2 , σ_C^2 , σ_E^2 and σ_M^2 can be obtained using the restricted likelihood maximum (ReML) algorithm [Patterson and Thompson, 1971; Harville, 1977; Lindstrom and Bates, 1988]. An estimate of heritability can be obtained by plugging ReML estimates of variance component parameters into Eq. (6). A standard error estimate of the heritability estimate can be obtained using a Taylor approximation and the information matrix of the variance component parameters when the ReML algorithm converges.

We note that when no repeat measurement is available, i.e., $n_i = 1$ for all i , we have $n = m$, $\mathbf{T} = \mathbf{I}_m$, and the model specified in Eqs. (4) and (5) becomes

$$\mathbf{y} = \mathbf{X} \boldsymbol{\beta} + \mathbf{g} + \mathbf{c} + \mathbf{e} + \boldsymbol{\epsilon}, \quad \text{cov}[\mathbf{y}] = \sigma_A^2 \mathbf{K} + \sigma_C^2 \boldsymbol{\Lambda} + \sigma_E^2 \mathbf{I}_m + \sigma_M^2 \mathbf{I}_m. \quad (7)$$

This model is unidentifiable because both the unique environmental factor \mathbf{e} and the intra-subject variation $\boldsymbol{\epsilon}$ are assumed to be normally distributed and independent across subjects. In this case, \mathbf{e} and $\boldsymbol{\epsilon}$ cannot be distinguished and have to be combined, leading to the classical ACE model (A: additive genetics; C: common environment; E: unique environment) for heritability analysis and the classical definition of heritability (i.e., the proportion of total phenotypic variation attributable to genetic variation). With repeat measurements, however, \mathbf{e} and $\boldsymbol{\epsilon}$ have different covariance structures ($\mathbf{T} \mathbf{T}^\top$ and \mathbf{I}_n , respectively), and thus can be modeled separately.

Simulation studies. We conducted simulation studies to ensure that our proposed method can robustly dissociate intra- and inter-subject variation of a phenotype and accurately estimate heritability due to inter-subject variation using repeat measurements. Specifically, we synthesized phenotypic data using the following model:

$$y_{ij} = \mathbf{x}_{ij}^\top \boldsymbol{\beta} + \gamma_i + \epsilon_{ij}, \quad \boldsymbol{\gamma} = [\gamma_1, \dots, \gamma_m]^\top = \mathbf{g} + \mathbf{c} + \mathbf{e}, \quad i = 1, 2, \dots, m, \quad j = 1, 2, \dots, n_i, \quad (8)$$

$$\boldsymbol{\beta} \sim \text{N}(\mathbf{0}, \mathbf{I}_q), \quad \mathbf{g} \sim \text{N}(\mathbf{0}, \sigma_A^2 \mathbf{K}), \quad \mathbf{c} \sim \text{N}(\mathbf{0}, \sigma_C^2 \boldsymbol{\Lambda}), \quad \mathbf{e} \sim \text{N}(\mathbf{0}, \sigma_E^2 \mathbf{I}_m), \quad \epsilon_{ij} \sim \text{N}(0, \sigma_M^2),$$

where we used real HCP covariates \mathbf{x}_{ij} , genetic similarity matrix \mathbf{K} , common environmental matrix $\mathbf{\Lambda}$, and number of repeat measurements n_i , and set $\sigma_A^2 = 0.8$, $\sigma_C^2 = 0.1$, $\sigma_E^2 = 0.1$ (i.e., the stable inter-subject variation was $\sigma_A^2 + \sigma_C^2 + \sigma_E^2 = 1$ and the heritability due to inter-subject variation was 0.8). We then added different levels of intra-subject variation σ_M^2 to the phenotypic data. The proportion of the total phenotypic variation (i.e., $\sigma_A^2 + \sigma_C^2 + \sigma_E^2 + \sigma_M^2$) due to intra-subject variation σ_M^2 ranged from 10% to 80%. For each level of the intra-subject variation, the simulation was repeat 1,000 times. We compared the heritability estimates due to inter-subject variation computed using our proposed method with the conventional heritability estimated by averaging repeat measurements for each individual and then applying the classical ACE model.

The Human Connectome Project (HCP). The HCP collects imaging, behavioral and demographic data from a large population of young and healthy adults and aims to shed light on anatomical and functional connectivity within the healthy human brain. In the present study, we analyzed 584 non-Hispanic/Latino European subjects (22-36 years) collected by the WU-Minn HCP Consortium. These subjects (age, 29.20 ± 3.47 years; female 55.99%) come from 247 families and comprise 72 MZ twin pairs, 67 DZ twin pairs, 251 full siblings of twins and 55 singletons (single birth individuals without siblings). Further details about the recruitment process and imaging data acquisition can be found in [Van Essen et al. \[2013, 2012\]](#); [Smith et al. \[2013\]](#); [Glasser et al. \[2013\]](#).

The Brain Genomics Superstruct Project (GSP). The Harvard/MGH Brain GSP is a neuroimaging and genetics study of brain and behavioral phenotypes. More than 3,500 native English-speaking adults with normal or corrected-to-normal vision were recruited from Harvard University, MGH and the surrounding Boston communities. Here we analyzed 809 unrelated young adults (18-35 years) of non-Hispanic European ancestry with no history of psychiatric illnesses or major health problems (age, 20.84 ± 2.77 years; female, 55.25%; right-handedness, 88.38%). All participants provided written informed consent in accordance with guidelines set by the Partners Health Care Institutional Review Board or the Harvard University Committee on the Use of Human Subjects in Research. For further details about the recruitment process, participants and imaging data acquisition, we refer the reader to [Holmes et al. \[2012, 2015\]](#).

Preprocessing of resting-state functional MRI data. We used MSM-All (areal feature based Multimodal Surface Matching algorithm [[Robinson et al., 2014](#)]) registered and ICA+FIX (FMRIB's ICA-based X-noiseifier [[Salimi-Khorshidi et al., 2014](#)]) denoised rs-fMRI data distributed by the WU-Minn HCP Consortium. MSM-All registration builds on FreeSurfer's folding-based surface registration [[Fischl, 2012](#)] and utilizes multivari-

ate areal features derived from myelin maps, resting-state network maps and rs-fMRI visuotopic maps in a joint multimodal registration to improve the alignment of cortical surface across subjects. FIX is an automatic noise detection and removal algorithm based on classification of spatial and temporal features generated from ICA (independent component analysis) of fMRI data. Among the 584 HCP subject we analyzed, 557 subjects had two rs-fMRI sessions on separate days and 27 subjects had one rs-fMRI session. Each rs-fMRI session consists of two scans of approximately 15 mins each with alternate phase encoding directions (left-to-right and right-to-left, respectively). For each scan, we smoothed the MSM-All registered and FIX denoised time series using a surface-based Gaussian kernel with 6 mm full width at half maximum (FWHM), and resampled the data to FreeSurfer’s *fsaverage5* representation, which consists of $n_{\text{vtx}} = 20,484$ vertices across the two hemispheres with an inter-vertex distance of approximately 4 mm. For each rs-fMRI session, we then standardized (subtracted the mean and divided by standard deviation) and concatenated the two scans.

The preprocessing of the GSP data involved (1) discarding the first four volumes of each scan to allow for T1-equilibration effects; (2) compensating for slice acquisition-dependent time shifts per volume with SPM2 (Wellcome Department of Cognitive Neurology, London, UK); and (3) correcting for head motion using rigid body translation and rotation with the FSL package [Jenkinson et al., 2002; Smith et al., 2009; Jenkinson et al., 2012]. Voxel-wise blood-oxygen-level dependent (BOLD) time series then underwent further preprocessing using procedures adapted from Biswal et al. [1995], and optimized for functional connectivity analysis. Briefly, constant offset and linear trend over each scan were removed and a temporal filter was applied to retain frequencies below 0.08 Hz. Sources of spurious variance, along with their temporal derivatives, were removed through linear regression, including (1) six parameters obtained by correction for rigid body head motion; (2) the signal averaged over the whole brain; (3) the signal averaged over the ventricles; and (4) the signal averaged over the deep cerebral white matter. GSP structural data were aligned as described in Yeo et al. [2011] using FreeSurfer [Fischl, 2012]. This technique yielded a surface mesh representation of the cortex from each participants structural scan, which was then registered to a common spherical coordinate system. Functional and structural images were then aligned to the common coordinate system by sampling from the middle of the cortical ribbon in a single interpolation step to reduce blurring of the functional signal across sulci and gyri. Additional details on the preprocessing procedures are outlined in Yeo et al. [2011]. All 809 GSP subjects had two rs-fMRI scans of approximately 6 mins each, acquired on the same model 12-channel head coil on separate days. Both scans had slice-based temporal signal-to-noise ratio (tSNR) greater than 100. We smoothed each scan using a surface-based Gaussian kernel with 6 mm FWHM and resampled the time series to FreeSurfer’s *fsaverage5* representation.

Computation of functional connectivity. For each HCP and GSP rs-fMRI scan, we computed an $n_{\text{vtx}} \times n_{\text{vtx}}$ Pearson correlation coefficient matrix using the preprocessed time series. The correlation coefficients were then spatially standardized (subtracted the mean and divided by standard deviation) into z-scores to make functional connectivity strength between each pair of vertices comparable across subjects. A previously published and widely used rs-fMRI-based parcellation of the cortex [Yeo et al., 2011] was used to summarize z-scores based on human corticocortical networks. Specifically, the 7-network parcellation obtained in [Yeo et al., 2011] was split into 51 spatially contiguous regions across the two hemispheres, and the z-scores were averaged within and across network regions into a 51×51 matrix.

Test-retest reliability. In the HCP sample, test-retest reliability of the network-level functional connectivity measurements (i.e., each average z-score in the 51×51 matrix) was computed as the Pearson correlation coefficient of z-scores from a subsample of 246 unrelated subjects who were selected from different families and had repeat rs-fMRI scans. In the GSP sample, test-retest reliability was computed similarly using all the 809 subjects who had repeat scans.

Heritability analysis. We estimated the non-transient heritability of each rs-fMRI-derived functional connectivity measurement in the 51×51 matrix in the HCP sample using our proposed LME model as specified in Eqs. (4) and (5) and the definition of heritability in Eq. (6), adjusting for age, gender and handedness as fixed-effect covariates. To benchmark our results, for each entry in the 51×51 matrix, we averaged measurements from repeat scans to obtain one scalar measurement for each subject, and then estimated the heritability using a classical ACE model, adjusting for age, gender and handedness as covariates.

We averaged heritability estimates of within-network functional connectivity measurements to obtain an overall heritability estimate for each of the 7 functional networks. To estimate the variance of the overall heritability estimate, we employed a block-jackknife procedure whereby each time one family was left out and the overall heritability was re-estimated using the subsample. This procedure was repeated for all the $n_{\text{fam}} = 247$ families to yield the jackknife heritability estimates $\hat{h}^2(k)$, $k = 1, 2, \dots, n_{\text{fam}}$. The variance of the overall heritability estimate was then estimated as [Efron and Tibshirani, 1994]

$$\text{var}[\hat{h}^2] = \frac{n_{\text{fam}} - 1}{n_{\text{fam}}} \sum_{k=1}^{n_{\text{fam}}} \left(\hat{h}^2(k) - \hat{h}^2(\cdot) \right)^2, \quad (9)$$

where $\hat{h}^2(\cdot) = \sum_{k=1}^{n_{\text{fam}}} \hat{h}^2(k) / n_{\text{fam}}$.

Analysis of the PCC seed-map. We used the MNI coordinates $[-3, -49, 25]$ reported in Yeo et al. [2011] as

the seed location in PCC, and found the vertex (MNI coordinates $[-2.917, -48.487, 24.970]$) in the *fsaverage5* system that has the shortest Euclidean distance to the seed. For each subject, the row in the $n_{\text{vtx}} \times n_{\text{vtx}}$ spatially standardized correlation coefficient matrix that corresponds to the selected vertex was then used as the functional connectivity profile of PCC. The test-retest reliability of this profile was computed similarly in the HCP sample as the test-retest reliability of the network-level functional connectivity measurements described above. The classical ACE model and the proposed LME model were used to estimate the heritability for each of the elements in the functional connectivity profile in the HCP sample. Surface maps of the heritability estimates were smoothed using a surface-based Gaussian kernel with 12 mm FWHM for visualization.

Acknowledgements

This research was carried out at the Athinoula A. Martinos Center for Biomedical Imaging at the Massachusetts General Hospital (MGH), using resources provided by the Center for Functional Neuroimaging Technologies, P41EB015896, a P41 Biotechnology Resource Grant supported by the National Institute of Biomedical Imaging and Bioengineering (NIBIB), National Institutes of Health (NIH). This work also involved the use of instrumentation supported by the NIH Shared Instrumentation Grant Program; specifically, grant numbers S10RR023043 and S10RR023401.

Data were provided in part by the Human Connectome Project (HCP), WU-Minn Consortium (principal investigators: David Van Essen and Kamil Ugurbil; 1U54MH091657) funded by the 16 NIH Institutes and Centers that support the NIH Blueprint for Neuroscience Research; and by the McDonnell Center for Systems Neuroscience at Washington University. Data were also provided in part by the Brain Genomics Superstructure Project (GSP) of Harvard University and MGH, with support from the Center for Brain Science Neuroinformatics Research Group, Athinoula A. Martinos Center for Biomedical Imaging, Center for Human Genetic Research and Stanley Center for Psychiatric Research. Twenty individual investigators at Harvard and MGH generously contributed data to the overall project.

This research was also funded in part by NIH grants R01NS083534, R01NS070963, and 1K25EB013649-01 (to MRS); K24MH094614 and R01MH101486 (to JWS); K01MH099232 (to AJH); an MGH ECOR Tosteson Postdoctoral Fellowship Award (to TG); and a BrightFocus Foundation grant AHAF-A2012333 (to MRS). JWS is a Tepper Family MGH Research Scholar.

References

- P.M. Visscher, W.G. Hill, and N.R. Wray. Heritability in the genomics era: concepts and misconceptions. *Nature Reviews Genetics*, 9(4):255–266, 2008.
- D.S. Falconer. *Introduction to quantitative genetics*. Oliver And Boyd; Edinburgh; London, 1960.
- M. Neale and L. Cardon. *Methodology for genetic studies of twins and families*. Springer, 1992.
- L. Almasy and J. Blangero. Multipoint quantitative-trait linkage analysis in general pedigrees. *The American Journal of Human Genetics*, 62(5):1198–1211, 1998.
- T.J.C. Polderman, B. Benyamin, C.A. De Leeuw, P.F. Sullivan, A. Van Bochoven, et al. Meta-analysis of the heritability of human traits based on fifty years of twin studies. *Nature Genetics*, 47(7):702–709, 2015.
- J. Yang, B. Benyamin, B.P. McEvoy, S. Gordon, A.K. Henders, et al. Common SNPs explain a large proportion of the heritability for human height. *Nature Genetics*, 42(7):565–569, 2010.
- J. Yang, S.H. Lee, M.E. Goddard, and P.M. Visscher. GCTA: a tool for genome-wide complex trait analysis. *The American Journal of Human Genetics*, 88(1):76–82, 2011.
- D. Golan, E.S. Lander, and S. Rosset. Measuring missing heritability: Inferring the contribution of common variants. *Proceedings of the National Academy of Sciences*, 111(49):E5272–E5281, 2014.
- T. Ge, T.E. Nichols, P.H. Lee, A.J. Holmes, J.L. Roffman, et al. Massively expedited genome-wide heritability analysis (MEGHA). *Proceedings of the National Academy of Sciences*, 112(8):2479–2484, 2015.
- T. Ge, M. Reuter, A.M. Winkler, A.J. Holmes, P.H. Lee, et al. Multidimensional heritability analysis of neuroanatomical shape. *Nature Communications*, 7:13291, 2016a.
- T. Ge, C. Chen, B.M. Neale, M.R. Sabuncu, and J.W. Smoller. Phenome-wide heritability analysis of the uk biobank. *bioRxiv*, page 070177, 2016b.
- G. Krüger and G.H. Glover. Physiological noise in oxygenation-sensitive magnetic resonance imaging. *Magnetic Resonance in Medicine*, 46(4):631–637, 2001.
- C. Triantafyllou, R.D. Hoge, G. Krueger, C.J. Wiggins, A. Potthast, et al. Comparison of physiological noise at 1.5 T, 3 T and 7 T and optimization of fMRI acquisition parameters. *NeuroImage*, 26(1):243–250, 2005.

- R.M. Hutchison, T. Womelsdorf, E.A. Allen, P.A. Bandettini, V.D. Calhoun, et al. Dynamic functional connectivity: promise, issues, and interpretations. *NeuroImage*, 80:360–378, 2013.
- S. Mueller, D. Wang, M.D. Fox, B.T.T. Yeo, J. Sepulcre, et al. Individual variability in functional connectivity architecture of the human brain. *Neuron*, 77(3):586–595, 2013.
- D.C. Glahn, A.M. Winkler, P. Kochunov, L. Almasy, R. Duggirala, et al. Genetic control over the resting brain. *Proceedings of the National Academy of Sciences*, 107(3):1223–1228, 2010.
- A. Fornito, A. Zalesky, D.S. Bassett, D. Meunier, I. Ellison-Wright, et al. Genetic influences on cost-efficient organization of human cortical functional networks. *The Journal of Neuroscience*, 31(9):3261–3270, 2011.
- P.M. Thompson, T. Ge, D.C. Glahn, N. Jahanshad, and T.E. Nichols. Genetics of the connectome. *NeuroImage*, 80:475–488, 2013.
- D.C. Van Essen, S.M. Smith, D.M. Barch, T.E.J. Behrens, E. Yacoub, et al. The WU-Minn human connectome project: an overview. *NeuroImage*, 80:62–79, 2013.
- A.J. Holmes, P.H. Lee, M.O. Hollinshead, L. Bakst, J.L. Roffman, et al. Individual differences in amygdala-medial prefrontal anatomy link negative affect, impaired social functioning, and polygenic depression risk. *The Journal of Neuroscience*, 32(50):18087–18100, 2012.
- A.J. Holmes, M.O. Hollinshead, T.M. OKeefe, V.I. Petrov, G.R. Fariello, et al. Brain Genomics Superstruct Project initial data release with structural, functional, and behavioral measures. *Scientific Data*, 2, 2015.
- B.T.T. Yeo, F.M. Krienen, J. Sepulcre, M.R. Sabuncu, D. Lashkari, et al. The organization of the human cerebral cortex estimated by intrinsic functional connectivity. *Journal of Neurophysiology*, 106(3):1125–1165, 2011.
- H.D. Patterson and R. Thompson. Recovery of inter-block information when block sizes are unequal. *Biometrika*, 58(3):545–554, 1971.
- D.A. Harville. Maximum likelihood approaches to variance component estimation and to related problems. *Journal of the American Statistical Association*, 72(358):320–338, 1977.
- M.J. Lindstrom and D.M. Bates. Newton-Raphson and EM algorithms for linear mixed-effects models for repeated-measures data. *Journal of the American Statistical Association*, 83(404):1014–1022, 1988.

- K.S. Kendler, L.M. Karkowski, and C.A. Prescott. Fears and phobias: reliability and heritability. *Psychological Medicine*, 29(3):539–553, 1999.
- R. Deichmann, J.A. Gottfried, C. Hutton, and R. Turner. Optimized EPI for fMRI studies of the orbitofrontal cortex. *NeuroImage*, 19(2):430–441, 2003.
- N. Weiskopf, C. Hutton, O. Josephs, and R. Deichmann. Optimal EPI parameters for reduction of susceptibility-induced BOLD sensitivity losses: a whole-brain analysis at 3 T and 1.5 T. *NeuroImage*, 33(2):493–504, 2006.
- J.D. Power, K.A. Barnes, A.Z. Snyder, B.L. Schlaggar, and S.E. Petersen. Spurious but systematic correlations in functional connectivity MRI networks arise from subject motion. *NeuroImage*, 59(3):2142–2154, 2012.
- K.R.A. Van Dijk, M.R. Sabuncu, and R.L. Buckner. The influence of head motion on intrinsic functional connectivity MRI. *NeuroImage*, 59(1):431–438, 2012.
- T.D. Satterthwaite, D.H. Wolf, J. Loughhead, K. Ruparel, M.A. Elliott, et al. Impact of in-scanner head motion on multiple measures of functional connectivity: relevance for studies of neurodevelopment in youth. *NeuroImage*, 60(1):623–632, 2012.
- M.P. van den Heuvel, I.L.C. van Soelen, C.J. Stam, R.S. Kahn, D.I. Boomsma, et al. Genetic control of functional brain network efficiency in children. *European Neuropsychopharmacology*, 23(1):19–23, 2013.
- R.L. Buckner, J.R. Andrews-Hanna, and D.L. Schacter. The brain’s default network. *Annals of the New York Academy of Sciences*, 1124(1):1–38, 2008.
- N.M. Laird and J.H. Ware. Random-effects models for longitudinal data. *Biometrics*, 38(4):963–974, 1982.
- G. Verbeke and G. Molenberghs. *Linear mixed models for longitudinal data*. Springer Science & Business Media, 2009.
- D.C. Van Essen, K. Ugurbil, E. Auerbach, D. Barch, T.E.J. Behrens, et al. The Human Connectome Project: a data acquisition perspective. *NeuroImage*, 62(4):2222–2231, 2012.
- S.M. Smith, C.F. Beckmann, J. Andersson, E.J. Auerbach, J. Bijsterbosch, et al. Resting-state fMRI in the human connectome project. *NeuroImage*, 80:144–168, 2013.

- M.F. Glasser, S.N. Sotiropoulos, J.A. Wilson, T.S. Coalson, B. Fischl, et al. The minimal preprocessing pipelines for the Human Connectome Project. *NeuroImage*, 80:105–124, 2013.
- E.C. Robinson, S. Jbabdi, M.F. Glasser, J. Andersson, G.C. Burgess, et al. MSM: A new flexible framework for Multimodal Surface Matching. *NeuroImage*, 100:414–426, 2014.
- G. Salimi-Khorshidi, G. Douaud, C.F. Beckmann, M.F. Glasser, L. Griffanti, et al. Automatic denoising of functional MRI data: combining independent component analysis and hierarchical fusion of classifiers. *NeuroImage*, 90:449–468, 2014.
- B. Fischl. Freesurfer. *NeuroImage*, 62(2):774–781, 2012.
- M. Jenkinson, P. Bannister, M. Brady, and S. Smith. Improved optimization for the robust and accurate linear registration and motion correction of brain images. *NeuroImage*, 17(2):825–841, 2002.
- S.M. Smith, P.T. Fox, K.L. Miller, D.C. Glahn, P.M. Fox, et al. Correspondence of the brain’s functional architecture during activation and rest. *Proceedings of the National Academy of Sciences*, 106(31):13040–13045, 2009.
- M. Jenkinson, C.F. Beckmann, T.E.J. Behrens, M.W. Woolrich, and S.M. Smith. FSL. *NeuroImage*, 62(2): 782–790, 2012.
- B. Biswal, F. Zerrin Yetkin, V.M. Haughton, and J.S. Hyde. Functional connectivity in the motor cortex of resting human brain using echo-planar MRI. *Magnetic Resonance in Medicine*, 34(4):537–541, 1995.
- B. Efron and R.J. Tibshirani. *An introduction to the bootstrap*. CRC press, 1994.